Complete Corrosion Inhibition through Graphene Defect Passivation

Ya-Ping Hsieh,[†,*] Mario Hofmann,[‡] Kai-Wen Chang,[†] Jian Gang Jhu,[†] Yuan-Yao Li,[†] Kuang Yao Chen,[§] Chang Chung Yang,[§] Wen-Sheng Chang,[§] and Li-Chyong Chen[⊥]

[†]Graduate Institute of Opto-Mechatronics, National Chung Cheng University, 168 University Road, Min-Hsiung Township, Chiayi County, Taiwan 62102, [‡]Department of Material Science and Engineering, National Cheng Kung University, Tainan, Taiwan 70101, [§]Green Energy and Environment Research Laboratories, Industrial Technology Research Institute, Hsinchu, Taiwan 31040, and [⊥]Center for Condensed Matter Sciences, National Taiwan University, Taipei, Taiwan 10617

ABSTRACT Graphene is expected to enable superior corrosion protection due to its impermeability and chemical inertness. Previous reports, however, demonstrate limited corrosion inhibition and even corrosion enhancement of graphene on metal surfaces. To enable the reliable and complete passivation, the origin of the low inhibition efficiency of graphene was investigated. Combining electrochemical and morphological characterization techniques, nanometer-sized structural defects in chemical vapor deposition grown graphene were found to be the cause for the limited passivation effect. Extremely fast mass transport on the order of meters per second both across and parallel to graphene layers results in an inhibition efficiency of only ~50% for Cu covered with up to three graphene layers. Through selective passivation of the defects by atomic layer deposition (ALD) an enhanced corrosion protection of more than 99% was achieved, which compares favorably with commercial corrosion protection methods.

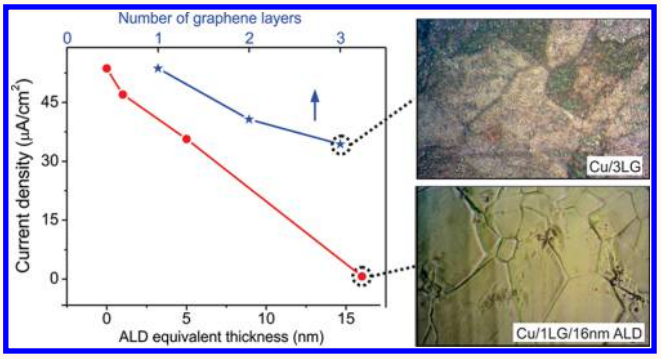

KEYWORDS: graphene · electrochemistry · defect · corrosion inhibition · passivation

Graphene, a two-dimensional carbon allotrope, has been heralded as an enabling material for a wide array of research fields ranging from electronics to biology.[1]

The use of graphene as a protective barrier could provide a starting point for the large-scale commercial application of graphene. For this goal, graphene is envisioned to act as a barrier that prevents mass transport between the environment and a metallic surface. Graphene-based protective layers could be used to prevent corrosive degradation of metallic surfaces, a market estimated to be ~$276 billion USD annually[2] and furthermore could provide environmental protection of unstable surfaces in different areas from biology[3] to spintronics.[4] Graphene has several advantages over current protection methods, such as inert metals, self-assembled monolayers,[5] or polymeric coatings,[6] including low cost, thermal and chemical stability, environmental friendliness, and high thermal and electric conductivity.[1] In addition to these superior characteristics, graphene's atomic thickness makes it transparent to light, electrons, and electrostatic interactions, which enables innovative uses of graphene that cannot be accomplished with traditional protection methods, for example, as vacuum-tight enclosures for biological imaging[7] and pressure sensing.[8]

Graphene's initially reported impermeability to gases[9] and oxidizers[10] added to the appeal of graphene as a perfect protective coating. Electrochemical corrosion experiments were the first to observe issues with this picture. Kirkland *et al.*[11] found that single-layer graphene did not protect Cu under anodic conditions. In later experiments researchers[12−14] observed a decrease in the corrosion rate between 85% and 95% for copper protected by single-layer graphene (subsequently denoted Cu/1LG), which remains inferior to organic and inorganic passivation layers.[15] Recent results indicate that even this limited corrosion resistance exists only for short-term corrosion experiments. Long-term exposure

* Address correspondence to yphsieh@ccu.edu.tw.

Received for review September 10, 2013 and accepted December 22, 2013.

Published online December 23, 2013
10.1021/nn404756q

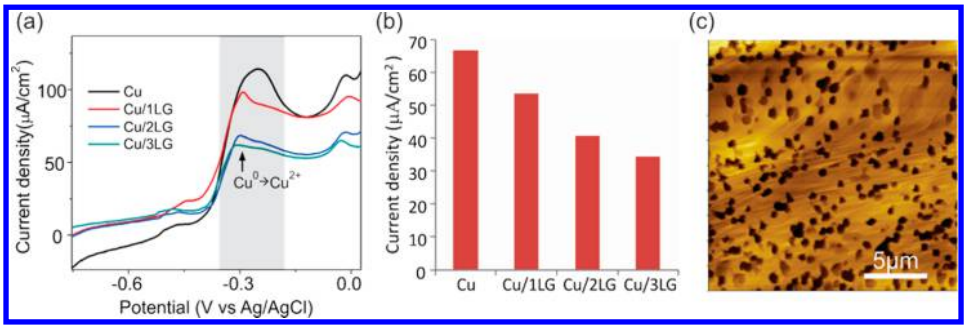

Figure 1. (a) Cyclic voltammogram of bare Cu and Cu passivated by 1−3 layers of graphene, (b) comparison of intensity of main oxidation peak under different passivation conditions, and (c) atomic force microscope image of Cu/graphene after etching.

studies instead found that graphene enhanced the corrosion of Cu[16,17] due to its cathodic character toward Cu in the presence of an electrolyte. Consequently, only a complete suppression of ionic conduction through the graphene can prevent the formation of a galvanic cell.

In light of these findings, the origin of the incomplete passivation has to be found and strategies for perfect passivation have to be identified. Previously, electrochemical measurements,[12,14] optical microscopy,[16,17] and comparison with multilayer graphene[12] were employed to correlate the inhibition efficiency of graphene with its structural quality. These studies suggested the presence of grain boundaries and openings in the graphene cause the observed incomplete passivation. These defects were attributed to growth conditions yielding polycrystalline[17] or discontinuous films[12] without attempting to further investigate this assertion.

We here use a combined approach of electrochemical analysis and morphological characterization to study the origin of the incomplete passivation effect of the Cu/graphene system. We demonstrate that nanometer-sized structural defects in the graphene are responsible for the limited passivation effect. Unprecedentedly high mass transport through microscopic graphene openings and along graphene layers is causing a maximum inhibition efficiency of 50% for the Cu/3LG system. Site-selective passivation of structural defects through atomic layer deposition was employed to estimate the dimensions of these openings and suppress permeation of liquid. Using this second passivation step, an inhibition efficiency of more than 99% was demonstrated for the first time, making the Cu/graphene/ALD system one of the best corrosion inhibitors reported.

RESULTS

Cyclic voltammetry was used to investigate the corrosion process, and several peaks can be observed in a cyclic voltammogram (Figure 1a) that are associated with the different oxidation states of copper during etching in agreement with previous reports.[18] The passivation effect of graphene is demonstrated by a decrease of the oxidation peaks since less ion exchange occurs. One prominent peak (as indicated in Figure 1a), representing the corrosion reaction of copper ($Cu^0 \rightarrow Cu^{2+} + 2e^-$), was chosen to quantify the passivation effect. The peak current is proportional to the charge exchanged, and we observe a decrease of only 20% upon passivation with one layer graphene (Cu/1LG).

Singh Raman *et al.*[13] attributed this limited passivation efficiency to the incomplete coverage of graphene with large areas of Cu remaining unprotected. To rule out this effect, we transferred multiple layers of graphene onto the Cu foil (Cu/2LG and Cu/3LG). This configuration would ensure that incomplete graphene layers are covered by subsequent transfers, and a higher value of total graphene coverage is expected. Previous reports indeed observed a significant improvement of the inhibition efficiency for an increasing number of transferred layers.[12] The inferior performance to multilayer graphene directly grown on the electrode was attributed to remaining openings.[12] From this model, the chance of finding an uncovered opening would decrease with the number of transferred layers according to the formula

$$T = 1 - \delta^N$$

where T is the density of uncovered openings, δ denotes the defect density per layer, and N is the number of layers. On the basis of this equation, the decrease of defects should be dramatic even if only one additional layer was transferred. Instead, Figure 1b shows that the decrease of the oxidation peak current is very limited even if three graphene layers are employed.

The almost linear decrease of corrosion current with number of layers suggests that the corrosion current is not controlled by the transport across the graphene barrier and instead mass transport between layers has to be considered.

To elucidate the reason for this low inhibition efficiency, we emulated the process of corrosion by exposing a Cu/graphene sample to APS copper

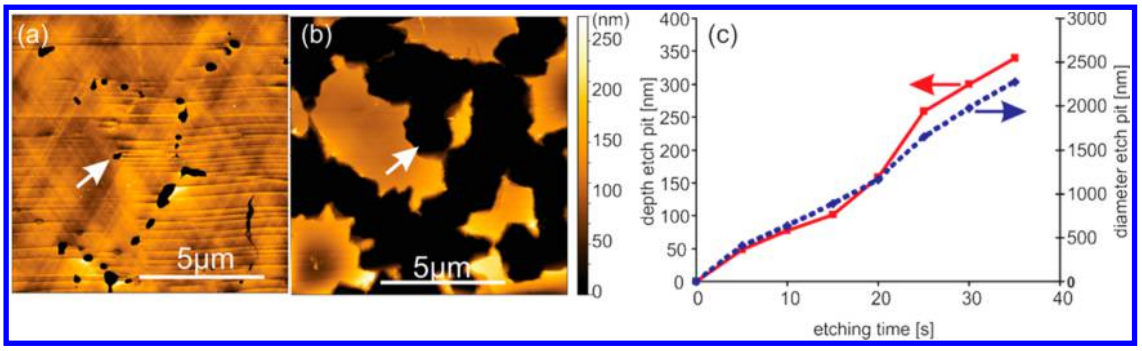

Figure 2. Cu/1LG morphology after (a) 5 s and (b) 35 s etching. (c) Dimensions (depth and diameter) of one etch pit as indicated in (a) and (b) *vs* etching time.

etchant since the process of APS etching can be precisely controlled. A multitude of etch pits can be seen from the atomic force microscope (AFM) image of the Cu/1LG sample (Figure 1c). The homogeneous occurrence of etch pits indicates that there are no regions that are free of graphene. Instead, the graphene itself seems to be porous and can be penetrated during the etching process. This observation agrees with previous studies of structural defects in graphene using atomic resolution imaging,[19] film-induced frustrated etching,[20] and oxidation methods.[21] Those studies have shown that an improved growth process can result in a decrease of the defect density, and we present results on the effect of growth optimization on inhibition efficiency in the Supporting Information (Suppl. Figure S1). However, neither previous reports nor our results have demonstrated a complete elimination of structural defects by growth optimization. Consequently, a better understanding of the fluid-dynamic properties of these defects has to be gained to predict their impact on graphene-based protective barriers.

Changes in the Cu morphology after exposure to an etchant were investigated by a series of AFM images that were taken at the same location after etching in 5 s intervals (Figure 2a,b). The change of etch pit dimensions with time can reveal the rate-limiting step of the etching process. If the etching is controlled by diffusive transport through the graphene orifice, a direct proportionality between the etch time t_{etch} and the etched volume is predicted by Kuiken[22] for small orifice sizes. Therefore the etch pit diameter and depth would scale with $(t_{etch})^{1/3}$. A linear increase of etch pit dimension with time, on the other hand, would be expected if the process was etch rate limited.

The observed linear proportionality of etch pit depth and diameter with time in Figure 2 suggests that the process is limited by the etch rate of the Cu. The measured increase in etch pit depth of 9 nm/s is indeed comparable to the etch rate of bare copper (Suppl. Figure S3).

The finding that the etching process is not transport limited even for etch pits of micrometer size is unusual but agrees with simulations by Suk *et al.*, who estimated the permeation speed of liquid through a graphene orifice to be up to 20 m/s.[18] This extraordinarily fast mass transport through graphene orifices can explain our previous results that the presence of almost complete graphene sheets is not significantly limiting the corrosion process. From the observed hole density of $\sim$1 um^{-2}, we estimate the permeation speed of reactant to be >1 m/s to result in the observed corrosion currents. (An alternative measurement process that arrives at a similar value is described in section 2 of the Supporting Information.)

Our time-resolved etching study also reveals another important fluid dynamic property of graphene. From Figure 2c the etch rate in the lateral direction is found to be $\sim$3$\times$ higher than perpendicular to the graphene membrane. An occurring higher etch rate along the graphene plane was previously observed in the fabrication of graphene devices[23] and efficient water permeation through graphene oxide films was found[24] and attributed to capillary action. This observation suggests that mass transport proceeds extremely fast not only across graphene membranes but also along the graphene plane, which was suggested previously by investigation of water permeation in thin films of graphene flakes.[24] This finding can explain our earlier observation that the passivation effect is not enhanced significantly when more graphene layers are used (Figure 1b). Due to the fast transport both along and across graphene layers, etchant can permeate through holes in the outer layer and then spread laterally to find a hole in the next layer.

Our demonstration of an extremely efficient mass transport through openings in the graphene layer raises questions about the size of these openings. Attempts to directly measure these dimensions, *i.e.*, through transmission electron microscopy (TEM), are hindered by several issues. First, there is an incongruence between the required resolution and image scale. Our studies suggest an average defect density of less than 1 nanosized defect per μm^2.[20] Therefore, dozens of high-resolution images would have to be taken to reveal one defect. Furthermore, structural defects are expected to cause dangling bonds that

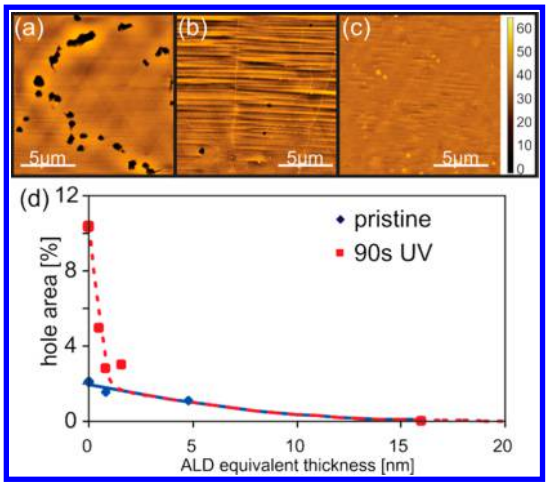

Figure 3. (a–c) Representative AFM height image of etched graphene (a) without, (b) with 5 nm ALD film, and (c) with 16 nm ALD film. (d) Copper hole area after deposition of ALD films for pristine and UV-ozone-treated graphene films.

lead to the formation of adsorbate clusters upon transfer,[25] which hinder high-resolution imaging.

To overcome these challenges, we have developed an indirect approach to measure the graphene hole size distribution directly on Cu based on atomic layer deposition (ALD). It was previously found[26] that deposition of atomic layers of aluminum oxide would preferentially occur at defects in the graphene lattice. Thus, aluminum oxide is expected to generate individual clusters on graphene rather than continuous films as on other surfaces. This observation agrees with AFM measurements that show the formation of ALD clusters with diameters that are similar to the expected equivalent film thickness (Figure 3b and c). Due to this cluster formation process, the electrochemical activity of graphene is not deteriorated by ALD passivation, as confirmed by its preserved ability to reduce hydrogen (Suppl. Figure S5). In contrast, ALD films of less than 5 nm thickness render bare Cu surfaces inert and unusable for electrochemical experiments (Suppl. Figure S7).

The sensitivity of ALD to dangling bonds results in the selective deposition of clusters on the edges of the holes in graphene. Furthermore, the large predicted interface resistance of graphene pores to gas transport[27] due to the multitude of intermediate steps will hinder permeation of gaseous precursor and atomic layer formation on the copper substrate. Since the formed aluminum oxide will etch at a significantly slower rate than copper,[28] the cluster starts presenting an etching barrier when it reaches the size of the graphene orifice. Thus, the dimension of the openings in the graphene can be inferred from the etching behavior of a sample as the thickness of the deposited ALD film is increased.

When comparing the defectiveness of identical graphene samples with and without 50 cycles of ALD (corresponding to ~5 nm equivalent film thickness) in Figure 3a and b, the effectiveness of aluminum oxide in suppressing the etching is demonstrated.

The comparison of Figure 3a–c shows the decrease in etch pit density with an increase in ALD film thickness, which allows identification of the occurring hole dimensions. Assuming that there is a distribution of orifices with different diameters, an ALD cluster of diameter d would cover and passivate all holes with a diameter smaller than a critical threshold dimension D. If the number of occurring hole sizes follows a Gaussian distribtion, the number of covered holes at a given ALD cluster size d are determined by the integral

$$N(d) = \int_0^d n_0 \exp\left(-\frac{(d-d_0)^2}{(C\delta)^2}\right) = n_0 \mathrm{erf}\left(\frac{d-d_0}{C\delta}\right)$$

Here C is a geometrical factor that relates the graphene hole dimension D and the ALD cluster size d. Assuming the cluster grows out symmetrically from dangling edge defects, a factor $C = 2$ can be used. The decrease in the number of uncovered holes will affect the etchant permeation and the etch rate $N(d)$. The agreement of the fit with the experimental data in Figure 3d suggests the validity of our simple model. To further confirm the appropriateness of the measuring method, a second experiment was performed: Exposure of graphene to ozone produced by decomposition of oxygen under ultraviolet light is known to generate lattice defects.[29] The higher etch rate N and the steeper slope of $N(d)$ confirm that UV ozone generates more defects with a smaller average diameter. From the fitting of $N(d)$ the hole size distribution in graphene can be analyzed. Under the presented assumptions we extract an average hole size of 1.6 nm for pristine graphene and 0.45 nm for ozone-generated holes. Despite the large errors associated with this simple model, these results highlight that nanometer-sized imperfections in the graphene limit its ability to passivate a surface. Consequently, suppressing permeation through the graphene openings is expected to significantly improve the performance of graphene-based passivation layers.

CV reveals a clear trend of a decreasing corrosion current for Cu/1LG/ALD systems with increasing ALD thickness (Figure 4a). Figure 4b shows the oxidation peak intensity of the $Cu^0 \rightarrow Cu^{2+}$ transition of Cu/graphene/ALD systems with different ALD thickness. It is evident that the ALD of 50 cycles (~5 nm equivalent thickness) renders the surface more inert that the transfer of three layers of graphene. Finally, the passivation effect achieved by 160 ALD cycles (~16 nm equivalent film thickness) results in an inhibition efficiency of >99%.

The large enhancement of the inhibition efficiency was also confirmed by Tafel analysis (Suppl. Figure S6). The corrosion rate of the Cu/1LG/16 nm ALD sample

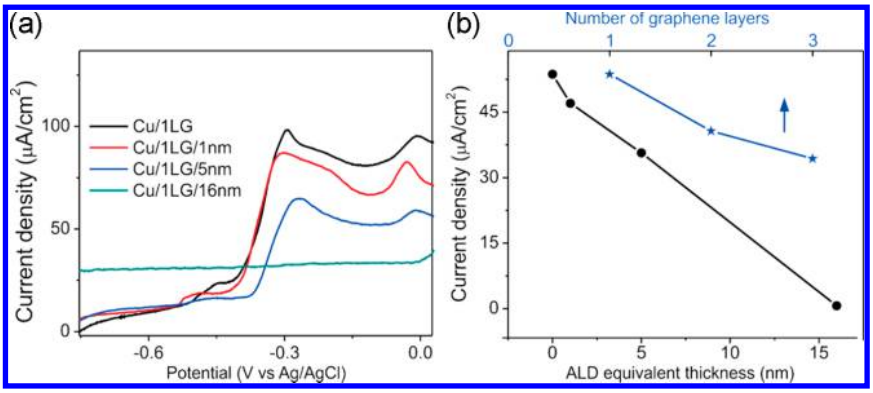

Figure 4. (a) CV spectra of Cu/graphene/ALD samples with different ALD thickness. (b) Peak current of Cu0 peak for Cu/graphene/ALD samples with different ALD thickness and comparison to peak current for Cu/graphene samples with 1−3 layers of graphene.

was measured to be 1.6×10^{-15} m/s, a 99% decrease compared to bare Cu and an 87% decrease compared to Cu/1LG. Finally, electrochemical impedance spectroscopy (EIS) suggests that the pore resistance associated with the graphene coverage increases by 65 times upon 16 nm ALD deposition (Suppl. Figure S7).

These values not only represent the highest reported inhibition efficiency for graphene-based passivation layers but are comparable to the best Cu corrosion inhibitors reported.[15] The importance of this progress is illustrated when comparing optical microscope images taken before and after CV experiments. It shows that after several hours of electrochemical etching conditions untreated Cu/graphene electrodes are severely damaged, whereas the Cu/graphene/ALD electrode exhibits a smooth surface (Suppl. Figure S8).

CONCLUSIONS

In conclusion, the incomplete passivation effect of graphene was found to be caused by structural defects in CVD-grown graphene. Extremely efficient mass transport both across and along graphene layers and through nanometer-sized openings was observed. By tuning the size of ALD-generated particles, the holes could be selectively passivated, which allowed inference to a hole diameter of 1.6 nm. Suppression of liquid permeation through these structural defects can enhance the performance of graphene as a corrosion inhibitor and enable the application of graphene-based passivation layers.

METHODS

Graphene was synthesized by chemical vapor deposition as previously reported[30] using copper as the catalyst material. Briefly, under low pressure (400 mTorr) a piece of copper foil (Alfa 13382) was annealed in a gas flow of 10 standard cubic centimeters (sccm) hydrogen at 1000 °C for 30 min before a flow of 20 sccm of methane gas was introduced to initiate the graphene growth. To control the graphene growth rate, 50 sccm of hydrogen was flowed during this period. After the synthesis process was completed the material was cooled under 5 sccm hydrogen to prevent oxidation and to minimize hydrogenation reactions of the graphene. The high quality was confirmed by electrical and spectroscopic characterization as detailed in the Supporting Information (Suppl. Figure S2).

Cyclic voltammetry was conducted on samples of 3×4 mm size using a potentiostat (CHI6081D), an Ag/AgCl reference electrode, and a Pt counter electrode. The electrolyte was aerated 0.1 M Na_2SO_4, and a standard scan rate of 10 mV/s was used in all experiments unless otherwise noted.

Atomic layer deposition was carried out in a homemade reactor at a base pressure of 1 Torr and a temperature of 100 °C. Trimethylaluminum (Sigma-Aldrich) and water were sequentially pulsed for 15 ms. N_2 was purged for 45 s after each precursor pulse to ensure equilibrium conditions.

Conflict of Interest: The authors declare no competing financial interest.

Acknowledgment. Y.H. acknowledges support under NSC-100-2112-M-194-006-MY3. M.H. acknowledges support under NSC-101-2112-M-006-017-MY3 and D102-33B07. K.C., C.Y., and W.C. acknowledge financial support from Bureau of Energy (Grant No.102-D0109), Ministry of Economic Affairs, Taiwan.

Supporting Information Available: Characterization of the graphene quality, measurements of the etching speed of bare Cu, characterization of ALD on graphene and Cu, electrochemical impedance analysis, Tafel analysis, and morphology of different passivated samples after long-term etching. This material is available free of charge *via* the Internet at http://pubs.acs.org.

REFERENCES AND NOTES

1. Novoselov, K.; Fal, V.; Colombo, L.; Gellert, P.; Schwab, M.; Kim, K. A Roadmap for Graphene. *Nature* **2012**, *490*, 192–200.
2. Thompson, N. G.; Yunovich, M.; Dunmire, D. Cost of Corrosion and Corrosion Maintenance Strategies. *Corros. Rev.* **2007**, *25*, 247–262.
3. Mohanty, N.; Fahrenholtz, M.; Nagaraja, A.; Boyle, D.; Berry, V. Impermeable Graphenic Encasement of Bacteria. *Nano Lett.* **2011**, *11*, 1270–1275.
4. Dlubak, B.; Martin, M.-B.; Weatherup, R. S.; Yang, H.; Deranlot, C.; Blume, R.; Schloegl, R.; Fert, A.; Anane, A.; Hofmann, S. Graphene-Passivated Nickel as an Oxidation-Resistant Electrode for Spintronics. *ACS Nano* **2012**, *6*, 10930–10934.
5. Sung, M. M.; Kim, Y. Self-Assembled Monolayers of Alkanethiols on Clean Copper Surfaces. *Bull. Korean Chem. Soc.* **2001**, *22*, 748–752.

6. Ahmad, N.; MacDiarmid, A. G. Inhibition of Corrosion of Steels with the Exploitation of Conducting Polymers. *Synth. Met.* **1996**, *78*, 103–110.
7. Yuk, J. M.; Park, J.; Ercius, P.; Kim, K.; Hellebusch, D. J.; Crommie, M. F.; Lee, J. Y.; Zettl, A.; Alivisatos, A. P. High-Resolution Em of Colloidal Nanocrystal Growth Using Graphene Liquid Cells. *Science* **2012**, *336*, 61–64.
8. Smith, A. D.; Niklaus, F.; Paussa, A.; Vaziri, S.; Fischer, A. C.; Sterner, M.; Forsberg, F.; Delin, A.; Esseni, D.; Palestri, P.; *et al.* Electromechanical Piezoresistive Sensing in Suspended Graphene Membranes. *Nano Lett.* **2013**, *13*, 3237–3242.
9. Bunch, J. S.; Verbridge, S. S.; Alden, J. S.; van der Zande, A. M.; Parpia, J. M.; Craighead, H. G.; McEuen, P. L. Impermeable Atomic Membranes from Graphene Sheets. *Nano Lett.* **2008**, *8*, 2458–2462.
10. Chen, S.; Brown, L.; Levendorf, M.; Cai, W.; Ju, S.-Y.; Edgeworth, J.; Li, X.; Magnuson, C. W.; Velamakanni, A.; Piner, R. D.; *et al.* Oxidation Resistance of Graphene-Coated Cu and Cu/Ni Alloy. *ACS Nano* **2011**, *5*, 1321–1327.
11. Kirkland, N. T.; Schiller, T.; Medhekar, N.; Birbilis, N. Exploring Graphene as a Corrosion Protection Barrier. *Corros. Sci.* **2012**, *56*, 1–4.
12. Prasai, D.; Tuberquia, J. C.; Harl, R. R.; Jennings, G. K.; Bolotin, K. I. Graphene: Corrosion-Inhibiting Coating. *ACS Nano* **2012**, *6*, 1102–1108.
13. Singh Raman, R. K.; Chakraborty Banerjee, P.; Lobo, D. E.; Gullapalli, H.; Sumandasa, M.; Kumar, A.; Choudhary, L.; Tkacz, R.; Ajayan, P. M.; Majumder, M. Protecting Copper from Electrochemical Degradation by Graphene Coating. *Carbon* **2012**, *50*, 4040–4045.
14. Ambrosi, A.; Bonanni, A.; Sofer, Z.; Pumera, M. Large-Scale Quantification of CVD Graphene Surface Coverage. *Nanoscale* **2013**, 2379–2387.
15. Hobbins, N. D.; Roberts, R. F. Copper Corrosion Inhibitor. US Patent 4,395,294, **1983**.
16. Zhou, F.; Li, Z.; Shenoy, G. J.; Li, L.; Liu, H. Enhanced Room-Temperature Corrosion of Copper in the Presence of Graphene. *ACS Nano* **2013**, *7*, 6939–6947.
17. Schriver, M.; Regan, W.; Gannett, W. J.; Zaniewski, A. M.; Crommie, M. F.; Zettl, A. Graphene as a Long-Term Metal Oxidation Barrier: Worse Than Nothing. *ACS Nano* **2013**, *7*, 5763–5768.
18. Suk, M. E.; Aluru, N. R. Water Transport through Ultrathin Graphene. *J. Phys. Chem. Lett.* **2010**, *1*, 1590–1594.
19. Tsen, A. W.; Brown, L.; Levendorf, M. P.; Ghahari, F.; Huang, P. Y.; Havener, R. W.; Ruiz-Vargas, C. S.; Muller, D. A.; Kim, P.; Park, J. Tailoring Electrical Transport across Grain Boundaries in Polycrystalline Graphene. *Science* **2012**, *336*, 1143–1146.
20. Hofmann, M.; Shin, Y.; Hsieh, Y.-P.; Dresselhaus, M.; Kong, J. A Facile Tool for the Characterization of Two-Dimensional Materials Grown by Chemical Vapor Deposition. *Nano Res.* **2012**, *5*, 504–511.
21. Duong, D. L.; Han, G. H.; Lee, S. M.; Gunes, F.; Kim, E. S.; Kim, S. T.; Kim, H.; Ta, Q. H.; So, K. P.; Yoon, S. J. Probing Graphene Grain Boundaries with Optical Microscopy. *Nature* **2012**, *490*, 235–239.
22. Kuiken, H. K. A Mathematical Model for Wet-Chemical Diffusion-Controlled Mask Etching through a Circular Hole. *J. Eng. Math.* **2003**, *45*, 75–90.
23. Du, X.; Skachko, I.; Barker, A.; Andrei, E. Y. Approaching Ballistic Transport in Suspended Graphene. *Nat. Nanotechnol.* **2008**, *3*, 491–495.
24. Nair, R. R.; Wu, H. A.; Jayaram, P. N.; Grigorieva, I. V.; Geim, A. K. Unimpeded Permeation of Water through Helium-Leak–Tight Graphene-Based Membranes. *Science* **2012**, *335*, 442–444.
25. Regan, W.; Alem, N.; Aleman, B.; Geng, B. S.; Girit, C.; Maserati, L.; Wang, F.; Crommie, M.; Zettl, A. A Direct Transfer of Layer-Area Graphene. *Appl. Phys. Lett.* **2010**, *96*, 113102.
26. Dai, H. J.; Wang, X. R.; Tabakman, S. M. Atomic Layer Deposition of Metal Oxides on Pristine and Functionalized Graphene. *J. Am. Chem. Soc.* **2008**, *130*, 8152–8153.
27. Drahushuk, L. W.; Strano, M. S. Mechanisms of Gas Permeation through Single Layer Graphene Membranes. *Langmuir* **2012**, *28*, 16671–16678.
28. Williams, K. R.; Gupta, K.; Wasilik, M. Etch Rates for Micromachining Processing-Part II. *J. Microelectromech. Syst.* **2003**, *12*, 761–778.
29. Tracz, A.; Wegner, G.; Rabe, J. P. Scanning Tunneling Microscopy Study of Graphite Oxidation in Ozone-Air Mixtures. *Langmuir* **2003**, *19*, 6807–6812.
30. Hsieh, Y.-P.; Wang, Y.-W.; Ting, C.-C.; Wang, H.-C.; Chen, K.-Y.; Yang, C.-C. Effect of Catalyst Morphology on the Quality of Cvd Grown Graphene. *J. Nanomater.* **2013**, *2013*, 393724.